Scalar collapse in AdS spacetimes

Alex Buchel, Luis Lehner, and Steven L. Liebling

Scalar Collapse in AdS

Alex Buchel,[1,2] Luis Lehner[1,3] and Steven L. Liebling[1,4]

[1] *Perimeter Institute for Theoretical Physics*
Waterloo, Ontario N2J 2W9, Canada

[2] *Department of Applied Mathematics*
University of Western Ontario
London, Ontario N6A 5B7, Canada

[3] *Department of Physics, University of Guelph*
Guelph, Ontario N1G 2W1, Canada

[4] *Department of Physics, Long Island University*
Brookville, NY 11548, U.S.A.

Abstract

Recently, studies of the gravitational collapse of a scalar field within spherically symmetric AdS spacetimes was presented in [1, 2] which showed an instability of pure AdS to black hole formation. In particular, the work showed that arbitrarily small initial configurations of scalar field evolved through some number of reflections off the AdS boundary until a black hole forms. We consider this same system, extended to include a complex scalar field, and reproduce this phenomena. We present tests of our numerical code that demonstrate convergence and consistency. We study the properties of the evolution as the scalar pulse becomes more compact examining the asymptotic behavior of the scalar field, an observable in the corresponding boundary CFT. We demonstrate that such BH formation occurs even when one places a reflecting boundary at finite radius indicating that the sharpening is a property of gravity in a bounded domain, not of AdS itself. We examine how the initial energy is transferred to higher frequencies –which leads to black hole formation– and uncover interesting features of this transfer.

1 Introduction

Two recent papers [1, 2] study the gravitational collapse of a real scalar field in spherically symmetric Anti-de Sitter (AdS) spacetimes finding a remarkable instability to black hole (BH) formation. That is, given any non-vanishing initial scalar field, they provide convincing numerical evidence, further supported by analytic arguments, that the resulting spacetime forms a BH within a time that scales inversely with the square of the initial amplitude of the scalar perturbation to AdS[1]. The work discussing this very interesting result, however, presents relatively few details and results from related work [4, 5] are in tension with it. We have therefore reproduced aspects of [1, 2] and provide new insights in this paper.

Such a result is, at first sight, surprising from a few different perspectives. Since Minkowski and de Sitter spacetimes are stable, it might be expected that AdS is stable as well [6]. Within the context of black hole critical phenomena [7, 8], the result is similarly surprising. In studies of critical behavior, one generally evolves a series of pulses with different amplitudes as the initial pulses implode through their centers, searching for the threshold of black hole formation. However, this instability suggests that a black hole is *always* formed and that this black hole threshold is only a threshold for *immediate* collapse.

In contrast, one can similarly view this instability from the perspective of the corresponding boundary conformal field theory (CFT). AdS-CFT asserts that BH solutions in the bulk correspond to thermal states of the CFT. In this light, the fact that this instability would always form a black hole would simply imply that states thermalize, which is not surprising at all. Furthermore, evidence for the instability has also been given in [9, 10] supporting this behavior based on ergodic arguments or linearized perturbation analysis as well as a theorem guaranteeing the instability under certain conditions [11]. On the other hand, recent works indicate that some scenarios never form a black hole, thus thermalization within the gauge/gravity context need not be a forgone conclusion [12, 13].

Furthermore, a pure state can never thermalize during a unitary evolution, and so the BH formation conjectures of [1, 2], as interpreted within the framework of AdS/CFT correspondence, indicate that it might be impossible to set-up a pure initial state in strict limit large-N gauge theories. Likewise, if the initial configuration carries a conserved global charge, one expects (at most) thermalization in a given charge sector. A global charge in the boundary CFT dynamics is realized through a local gauge symmetry of the dual gravitation bulk dynamics. We postpone the study of thermal-

---

[1]It is interesting to note that Pretorius & Choptuik foresaw this possibility in their study in $2 + 1$ AAdS [3].

ization of charged configurations in AdS to future work, and discuss here the effect of global symmetries in the bulk on the thermalization. To this end we extend the work of [1, 2] to a complex scalar field collapse in AdS.

This work is organized as follows; formulation of the problem is given in Section 2. We present a number of details of our numerical work in Section 3 and provide tests that our code produces convergent and consistent solutions through a number of reflections off the boundary. We consider the results of our simulations in Section 4, extending to a complex scalar field. In Section 5 we interpret the results of our simulations in a context of a dual boundary conformal gauge theory dynamics. We conclude in Section 6.

2 Formulation

Consider a $(d+1)$-dimensional gravitational system, dual to a strongly coupled CFT_d on $(d-1)$-dimensional sphere S^{d-1}. We focus on $SO(d)$-invariant states of a conformal field theory with nonzero expectation values for a pair of exactly marginal operators $\mathcal{O}_d^{(i)}$, $i = 1, 2$. We are interested in a unitary evolution of such states as determined by the following dual effective gravitational action

$$S_{d+1} = \frac{1}{16\pi G_{d+1}} \int_{\mathcal{M}_{d+1}} d^{d+1}\xi \sqrt{-g} \left(R_{d+1} + \frac{d(d-1)}{\ell^2} - 2\partial_\mu \phi \partial^\mu \phi^* \right), \quad (2.1)$$

where $\phi \equiv \phi_1 + i\,\phi_2$ is a massless complex scalar field, dual to a pair of exactly marginal operators $\mathcal{O}_d^{(1)} + i\,\mathcal{O}_d^{(2)} \equiv \mathcal{O}_d$. Further,

$$\mathcal{M}_{d+1} = \partial\mathcal{M}_{d+1} \times \mathcal{I}, \qquad \partial\mathcal{M}_{d+1} = R_t \times S^{d-1}, \qquad \mathcal{I} = \{x \in [0, \frac{\pi}{2}]\}. \quad (2.2)$$

Notice that the effective action (2.1) is invariant under a global phase rotation

$$\phi \to \phi\, e^{-i\alpha}, \quad (2.3)$$

corresponding to a phase rotation of expectation values

$$\langle \mathcal{O}_d \rangle \to \langle \mathcal{O}_d \rangle\, e^{-i\alpha}. \quad (2.4)$$

Associated with (2.3) there is a conserved current

$$J^\mu = ig^{\mu\nu} \left(\phi \partial_\nu \phi^* - \phi^* \partial_\nu \phi \right), \quad (2.5)$$

and a corresponding conserved charge

$$Q = \int_{S^{d-1}} dS^{d-1} \int_0^{\pi/2} dx\ \sqrt{-g} J^t. \quad (2.6)$$

3

The other conserved quantity of a CFT during the evolution is the total mass M. We can rephrase the work [1, 2] as a statement that nonequilibrium states $\{M, Q = 0\}$ of a strongly coupled CFT with a gravitational dual evolve into thermal states. Here, in addition to reproducing these claims (and reinterpreting the gravitational bulk dynamics from the boundary CFT perspective), we are interested in a broader question: *what is the role of a non-zero charge Q in the process of thermal equilibration?* Such a question is particularly interesting as it is well-known that a complex scalar field in AdS supports perturbatively-stable boson star solutions [14].

To proceed, we adopt a notation similar to that of [2] choosing the same form of the $(d + 1)$-dimensional metric describing an asymptotically AdS spacetime

$$ds^2 = \frac{\ell^2}{\cos^2 x} \left(-Ae^{-2\delta}dt^2 + \frac{dx^2}{A} + \sin^2 x \, d\Omega_{d-1}^2 \right) , \qquad (2.7)$$

where ℓ is the scale-size of the AdS spacetime, $d\Omega_{d-1}^2$ is the metric of S^{d-1}, and $A(x, t)$ and $\delta(x, t)$ are scalar functions describing the metric. The scale ℓ drops out of the resulting equations and we set it to unity without loss of generality. The spatial coordinate x runs over $0 \rightarrow \pi/2$ such that spheres through the point x have a radius $r \equiv \tan x$. To describe the real and imaginary components of a scalar field, we introduce the two quantities $\Phi_i \equiv (\partial/\partial x)(\phi_i)$ and $\Pi_i \equiv A^{-1}e^\delta (\partial/\partial t)(\phi_i)$.

Besides the extension from a real scalar to a complex scalar field, this is precisely as described in [2] and we derive the same equations of motion. However, working with these variables, achieving a stable numerical scheme required a few numerical tweaks at the outer boundary to provide convergent evolutions even through reflections (or bounces). A more elegant solution, and one which requires no such tricks, involves rescaling the matter functions in keeping with their appropriate boundary fall-off. In particular, we use rescaled quantities according to

$$\hat{\phi}_i \equiv \frac{\phi_i}{\cos^{d-1} x} , \qquad (2.8)$$

$$\hat{\Pi}_i \equiv \frac{e^\delta}{A} \frac{\partial_t \phi_i}{\cos^{d-1} x} = \frac{\Pi_i}{\cos^{d-1} x} , \qquad (2.9)$$

$$\hat{\Phi}_i \equiv \frac{\partial_x \phi_i}{\cos^{d-2} x} = \frac{\Phi_i}{\cos^{d-2} x} . \qquad (2.10)$$

In terms of these rescaled quantities (we drop the caret from here forward), we have the following evolution equations resulting from the Klein-

Gordon equation

$$\dot{\phi}_i = A e^{-\delta} \Pi_i \,,$$

$$\dot{\Phi}_i = \frac{1}{\cos^{d-2} x} \left(\cos^{d-1} x A e^{-\delta} \Pi_i \right)_{,x} \,,$$ (2.11)

$$\dot{\Pi}_i = \frac{1}{\sin^{d-1} x} \left(\frac{\sin^{d-1} x}{\cos x} A e^{-\delta} \Phi_i \right)_{,x} \,.$$

The system also includes two spatial equations to be integrated

$$A_{,x} = \frac{d - 2 + 2 \sin^2 x}{\sin x \cos x} (1 - A) - \sin x \cos^{2d-1} x A \left(\frac{\Phi_i^2}{\cos^2 x} + \Pi_i^2 \right) \,,$$

$$\delta_{,x} = - \sin x \cos^{2d-1} x \left(\frac{\Phi_i^2}{\cos^2 x} + \Pi_i^2 \right) \,,$$ (2.12)

together with one constraint equation

$$A_{,t} + 2 \sin x \cos^{2d-2} A^2 e^{-\delta} (\Phi_i \Pi_i) = 0 \,,$$ (2.13)

where a sum over $i = \{1, 2\}$ is implied.

At the origin, these quantities behave independently of d as

$$\phi_i(t, x) = \phi_0^{(i)}(t) + \mathcal{O}(x^2) \,,$$
$$A(t, x) = 1 + \mathcal{O}(x^2) \,,$$ (2.14)
$$\delta(t, x) = \delta_0(t) + \mathcal{O}(x^2) \,.$$

At the outer boundary $x = \pi/2$ we introduce $\rho \equiv \pi/2 - x$ so that we have

$$\phi_i(t, \rho) = \phi_d^{(i)}(t) \rho + \mathcal{O}(\rho^3) \,,$$
$$A(t, \rho) = 1 - M \frac{\sin^d \rho}{\cos^{d-2} \rho} + \mathcal{O}(\rho^{2d}) \,,$$ (2.15)
$$\delta(t, \rho) = 0 + \mathcal{O}(\rho^{2d}) \,.$$

We note here a difference between our work and [2]. We choose conditions on δ such that it becomes zero on the boundary and hence the coordinate time with which we examine the boundary describes proper time there as well. The gauge freedom in this system allows for such a rescaling without affecting the dynamics observed.

The asymptotic behavior (2.15) determines the boundary CFT observables: the expectation values of the stress-energy tensor T_{kl}, and the operators $\mathcal{O}_d^{(i)}$

$$8\pi G_{d+1} \langle T_{tt} \rangle = \mathcal{E}_d \,, \qquad \langle T_{\alpha\beta} \rangle = \frac{g_{\alpha\beta}}{d-1} \langle T_{tt} \rangle \,,$$

$$16\pi G_{d+1} \langle \mathcal{O}_d^{(i)} \rangle = 4d \, \phi_d^{(i)}(t) \,,$$ (2.16)

where $\mathcal{E}_d$, up to an additive constant[2] for even d, is proportional to M; $g_{\alpha\beta}$ is a metric on a round S^{d-1}. Explicitly, for $d = 3, 4$ we have

$$\mathcal{E}_d = \begin{cases} M , & d = 3 , \\ \frac{3}{8}(1 + 4M) , & d = 4 . \end{cases} \tag{2.17}$$

Additionally note that the conserved $U(1)$ charge is given by

$$Q = 4\pi^2 \int_0^{\pi/2} dx \ \sin^{d-1} x \ \cos^{d-1} x \ (\Pi_1(0, x)\phi_2(0, x) - \Pi_2(0, x)\phi_1(0, x)) . \tag{2.18}$$

Note that since $\partial_t Q = 0$, the integral in (2.18) can be evaluated at $t = 0$.

The constraint (2.13) implies that M in (2.15) is time-independent, ensuring energy conservation

$$\partial_t \ \mathcal{E}_d = 0 . \tag{2.19}$$

It is convenient to introduce the mass aspect function $\mathcal{M}(t, x)$ as

$$A(t, x) = 1 - \mathcal{M}(t, x)\frac{\cos^d x}{\sin^{d-2} x} . \tag{2.20}$$

Following (2.12) we find

$$\mathcal{M}(t, x) = \int_0^x dz \ \tan^{d-1} z \ \cos^{2(d-1)} z \ A(t, z) \left[\frac{\Phi_i^2(t, z)}{\cos^2 z} + \Pi_i^2(t, z)\right] . \tag{2.21}$$

Comparing (2.21) and (2.15) we see that

$$M = \mathcal{M}(t, x)\Big|_{x=\frac{\pi}{2}} . \tag{2.22}$$

Both $\mathcal{E}_d$ and the charge Q are determined from the initial data. Motivated by [1], in this paper we consider the following set of initial conditions:

■ $Q = 0$ case

$$\Phi_i(0, x) = 0 , \qquad \Pi_i(0, x) = \frac{2\epsilon}{\pi}e^{-\frac{4\tan^2 x}{\pi^2 \sigma^2}} \cos^{1-d} x \ \delta_i^1 , \tag{2.23}$$

where here δ_k^j represents the Kronecker delta. Numerically solving the spatial ODEs of (2.20) and (2.21), we compute $\mathcal{M}(0, \pi/2) = M$. For $d = 3\cdots 6$ and $\sigma = \frac{1}{16}$ the values $M(\epsilon)$ are presented in Fig. 1.

■ $Q \neq 0$ case

$$\Phi_i(0, x) = \partial_x \left[\frac{2\epsilon}{\pi}e^{-\frac{4\tan^2 x}{\pi^2 \sigma^2}} \cos^{1-d} x \ \delta_i^1\right] ,$$

$$\Pi_i(0, x) = \omega_d \frac{2\epsilon}{\pi}e^{-\frac{4\tan^2 x}{\pi^2 \sigma^2}} \cos^{1-d} x \ \delta_i^2 , \qquad \omega_d = d , \tag{2.24}$$

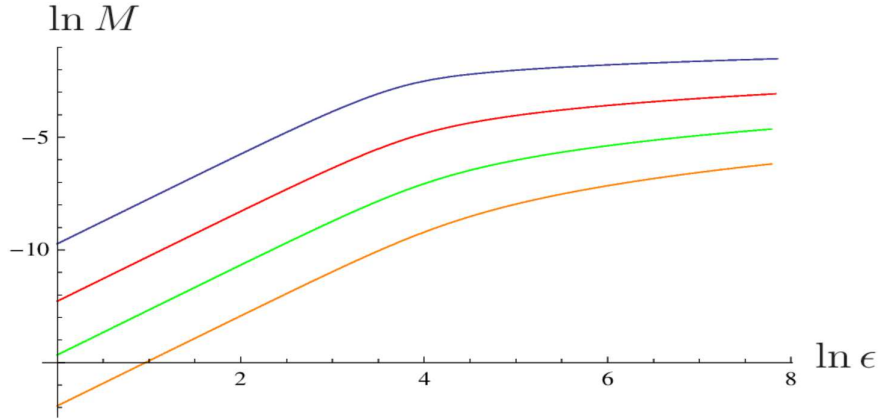[2]This constant determines the Casimir energy of the CFT$_d$.

6

Figure 1: Mass M of initial configurations (2.23) as a function of ϵ for $d = 3, 4, 5, 6$ (blue/red/green/orange curves). Note that $M \propto \epsilon^2$ for $\ln \epsilon \lesssim 4$. While the coordinate extent of the scalar profile is the same in all d, higher dimensional AdS_{d+1} more efficiently "localizes" it, resulting in smaller M_d for a fixed ϵ.

where ω_d is the lowest frequency of the linearized scalar perturbations of AdS_{d+1}. Numerically solving the spatial ODEs of (2.20) and (2.21), we compute $\mathcal{M}(0, \pi/2) = M$. For $d = 3 \cdots 6$ and $\sigma = \frac{1}{16}$, the values $M(\epsilon)$ and $\frac{M}{Q}$ are presented in Fig. 2.

Note that for both classes of initial conditions, (2.23) and (2.24), the values $\phi_d^{(i)}(0)$, and correspondingly the expectation values of the boundary CFT operators $\mathcal{O}_d^{(i)}$ at $t = 0$, are zero.

3   Numerics

3.1   Implementation

To solve these equations, we employ finite-difference approximations within a method-of-lines (MOL) approach that employs a third-order accurate Runge-Kutte (RK3) time evolution scheme. Such an approach computes the spatial derivatives (with a high-order accurate, finite-difference stencil) and then considers the evolution equations as ordinary-differential equations (ODEs) in the time coordinate.

As is standard in studies of critical behavior, we use adaptive mesh refinement (AMR) to add resolution where needed and remove it when not
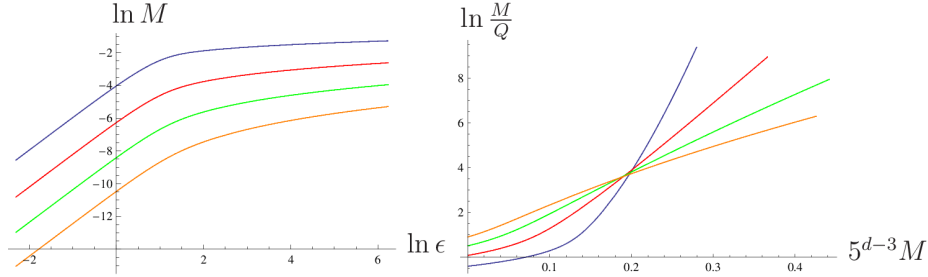
7

Figure 2: Mass M of initial configurations (2.24) as a function of ϵ for $d = 3 \cdots 6$ (left panel, blue $\cdots$ orange) and corresponding ratios $\frac{M}{Q}$ (right panel). Here, $M \propto \epsilon^2$ scaling of mass extends only up to $\ln \epsilon \sim 1$. Note that $\frac{M}{Q}$ approaches a constant as $M \to 0$, while $\ln \frac{M}{Q} \propto M$ for large M, effectively making the charge negligible. The rescaling of the horizontal axis of the right panel by 5^{d-3} is made for readability of the graph.

needed. In particular, we use Choptuik's `ad` infrastructure [7, 15] adapted for our uses here via the changes:

- modified the loop for convergence within the iterative Crank-Nicholson scheme to a three-step RK3 update

- replaced second-order accurate spatial derivatives with high-order accuracy spatial derivatives

- modified the AMR-boundary treatment from interpolation for a single point in time to interpolation in time of width two points in the parent, with spatial interpolation on the fine level between these two points. This approach follows in spirit the tapered approach of [16], although it strictly lacks the higher-order convergence there.

The numerical grid has two boundaries, the origin and the AdS boundary at $\rho \equiv \pi/2 - x = 0$. To enforce the boundary conditions (2.14) at the origin, we set $\Phi_i(t, 0) = 0$ and $A(t, 0) = 1$ and obtain values for $\phi_i(t, 0)$ and $\Pi_i(t, 0)$ from quadratic fits. Because $\delta(t, x)$ is computed by numerical integration from the outer boundary, no boundary condition is needed at the origin. At the $\rho = 0$ boundary, we enforce the conditions (2.15) by setting $\phi_i(t, \pi/2)$, $\Pi_i(t, \pi/2)$, and $\Phi_i(t, \pi/2)$ all to zero there. We set the metric functions $A(t, \pi/2) = 1$ and $\delta(t, \pi/2) = 0$, the latter chosen to ensure that coordinate time t measures proper time on the boundary.

3.2 Tests

We carry-out a number of tests of our implementation. We find that the solutions obtained generally converge at least as fast as third-order in the grid spacing. We evaluate the residual of the momentum constraint and confirm that it approaches zero as the resolution is increased. We compute both the total mass $\mathcal{M}(t, \pi/2)$ using (2.21) and charge using (2.18), and ensure that their degree of conservation in time improves with resolution. We also completed two standard black hole threshold searches and find the expected Choptuik behavior [7]. Fig. 3 presents some results from one such test. For the AMR evolutions mentioned here, we ensure that increasing both the coarse level resolution and decreasing the threshold for refinement produce essentially unchanged collapse times.

4 Results

We find the same behavior as found in [1, 2]. In particular, given any initial, non-vanishing configuration of scalar field, an evolution with sufficient resolution and time produces a black hole. We observe that as the pulse travels back and forth from the boundary, one sees increasing compactness in the scalar profile. Examining the metric function $A(x, t)$, one sees that on return of the pulse to the centre, the metric function approaches 0 to an increasing degree, and it is precisely the approach of $A(x, t)$ to zero that indicates the formation of a black hole. In other words, the increasingly compact scalar profile produces an increasingly deeper gravitational potential well. The location of this minimum also decreases with each bounce. We plot these two quantities in Fig. 4 for one particular run of the initial data of (2.23).

4.1 The Nature of the Instability

One can ask whether this instability results from the particular nature of AdS spacetime or instead just the fact that one is evolving in an essentially bounded domain. Beyond the perturbative analysis, one can imagine sending a scalar pulse down an elevator shaft equipped with a mirror. It will blueshift as it gets deeper, but upon return to its original height, it would obtain its original form only to first order. At higher order, one considers not just the gravity of the Earth, but also the self-gravity of the pulse which will act to compress the pulse to its center.

One could confirm this picture by numerically evolving a scalar pulse in an asymptotically flat space but with a reflecting boundary at some radius, as done in [17]. Instead, we do something similar but with our same code. That is, we enforce reflecting boundary conditions on the scalar field at some
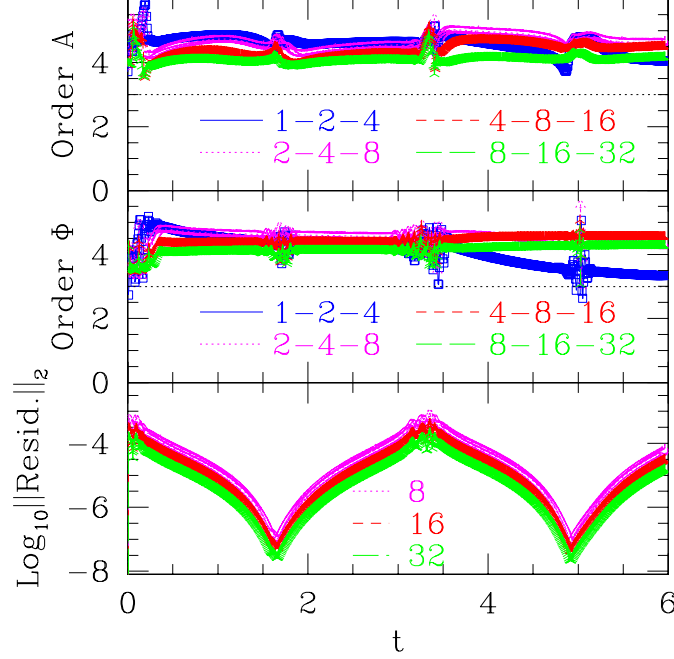
Figure 3: Convergence test for two bounces with $d = 3$. The initial data is of the form (2.23) with $\epsilon = 20.01$ and $\sigma = 1/16$. (**top**) The order of convergence obtained from comparisons of the metric function $A(x,t)$ at successively doubled resolutions. The convergence order is computed from three different resolutions, a base resolution and runs with half and one-quarter the base grid solution. Thus, run "32" has a grid spacing 2^{-5} that of the run labeled "1."(**middle**) Order of convergence obtained for $\Phi_1(x,t)$. Both these results indicate convergence is better than third order convergent. (**bottom**) The logarithm of the L2-norm of the momentum constraint residual for just the three best resolutions. That it decreases with increasing resolution suggests the results are converging to a proper solution of Einstein's equations. Note that this residual is computed only at first order of accuracy because it involves a time derivative and therefore one should *not* estimate the order of convergence from it.

10

$x_{\text{finite}} < \pi/2$

$$\phi_i(x_{\text{finite}}, t) = 0\,, \qquad \Pi_i(x_{\text{finite}}, t) = 0\,. \qquad (4.1)$$

The value is arbitrary, but by truncating the domain, the scalar pulse does not "see" that the spacetime in which it lives is AdS. We choose $x_{\text{finite}} = \pi/4$ and find that pulses behave qualitatively in the same way, i.e. as they bounce, they shift to shorter wavelengths and eventually form black holes. We subsequently varied the value of x_{finite} and confirmed that this behavior is robust. Interestingly when ϵ in initial data of the form (2.23) was decreased below 18.39, collapse was not observed even after hundreds of bounces.

4.2   Boundary Information

Given the AdS-CFT correspondence, it is interesting to consider what the boundary CFT sees from the bulk. One usually uses a "dictionary" to extract various quantities. However, here the boundary stress-energy tensor is time-independent and just equal to the total mass of the spacetime, M. Of particular relevance is the leading asymptotic value of the scalar field ϕ_i as its behavior corresponds to a quantum operator on the boundary. We therefore determine the asymptotic behavior of each scalar field ϕ_i with a polynomial, least-squares fit to

$$\phi_i(\rho, t) = \phi_d^{(i)}(t)\ \rho + \phi_{d+2}^{(i)}(t)\ \rho^3. \qquad (4.2)$$

As a check of our extracted value, we employ from ten to thirty points and confirm the results of the relevant quantity, $\phi_d^{(i)}(t)$ are hardly affected.

This asymptotic information is displayed for a particular case in Fig. 5. The left side shows the behavior as a function of time with each successive bounce along with the Fourier power spectrum. This spectrum is computed using the FFTW library [18] acting on $\phi_3^{(1)}(t)$ once it has been interpolated onto a uniform grid over t (recall the use of AMR produces nonuniform in time information for the asymptotic behavior). The power is computed as simply the square of the (complex) Fourier amplitude.

5   Boundary CFT perspective of the gravitational collapse

The formation of an apparent horizon (AH) in AdS gravitational collapse is holographically dual to the thermalization of an initial CFT state corresponding to the initial condition of the gravitational evolution. To fully characterize the gravitational dynamics from the boundary perspective, one would have to compute an infinite set of local correlation functions[3]. Here,

---

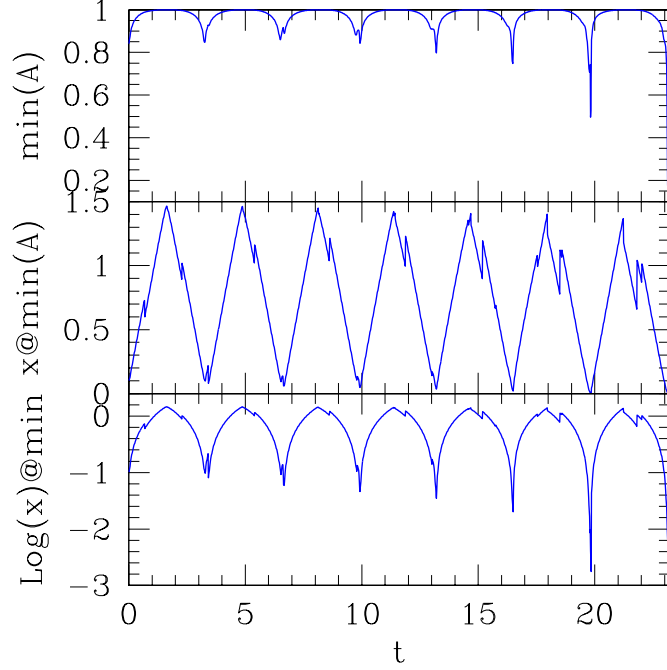[3]Also, presumably, the nonlocal observables such as Wilson loops.

Figure 4: Demonstration of the increasingly compact gravitational poten-
tial with successive bounces of initial data of form (2.23) with $\epsilon = 20$ and
$\sigma = 1/16$. Six bounces are shown before a black hole forms. (**top**) The
minimum of $A(x, t)$ as a function of time. At the final time, the minimum
approaches zero, signaling black hole formation. (**middle**) The x-coordinate
where $A(x, t)$ achieves its minimum. In these coordinates, the speed of light
is unity, and the line segments roughly indicate the motion of the scalar pulse
back and forth across the grid. That compaction increases with each bounce
is quite hard to observe on the linear scale, and so the logarithm of this data
is shown at **bottom**. The evolution terminates at the last time shown as the
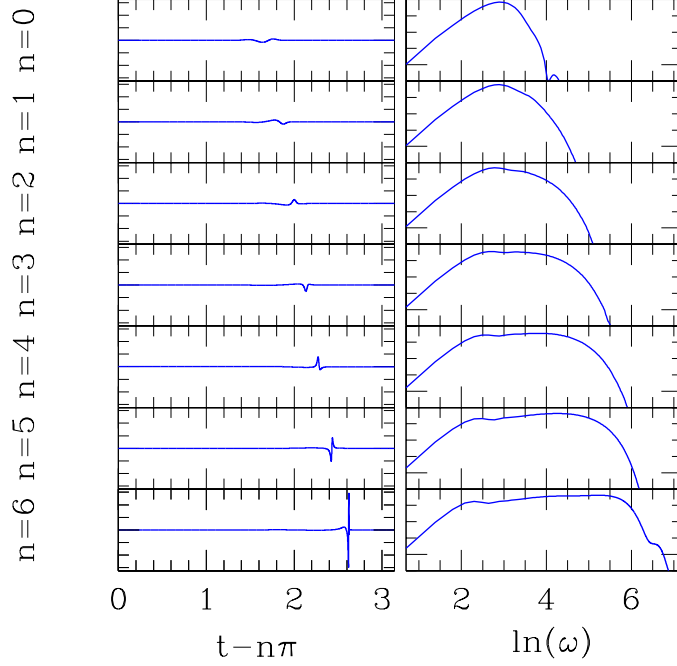solution approaches black hole formation.

Figure 5: The behavior of the scalar field at the boundary with successive bounces for the same evolution as in Fig. 4. At **left**, the asymptotic value $\phi_3^{(1)}(t)$ from Eq. (4.2) is shown for segments of time of length π. The pulse sharpens with each "implosion" through the origin. On the **right** is shown the Fourier transform of the signal on the left. Shown is the natural logarithm of the amplitude of the Fourier component squared as a function of (the log of) angular frequency ω. The vertical scale is arbitrary but fixed for all bounces. The transform shows that energy is shifted to higher frequencies.

13

we focus on the simplest local observables, namely $\langle \mathcal{O}_d^{(i)} \rangle \propto \phi_d^i$. Recall that the one-point function of the boundary stress-energy tensor is constant during the evolution (see (2.16)), and thus does not carry any information about AH formation. The same applies to the conserved $U(1)$ charge and so its role is to identify (select) dynamical thermalization trajectories.

5.1   Weakly nonlinear perturbations with global charge in AdS

Following [1] (see also [6]) we consider the solution of (2.11)-(2.13), perturbative in the bulk scalar amplitudes ϵ

$$\phi_i = \sum_{j=0}^{\infty} \epsilon^{2j+1} \, \phi_{i,2j+1} \,, \qquad A = 1 - \sum_{j=1}^{\infty} \epsilon^{2j} \, A_{2j} \,, \qquad \delta = \sum_{j=1}^{\infty} \epsilon^{2j} \, \delta_{2j} \,, \quad (5.1)$$

where $\phi_{i,2j+1}$, A_{2j}, δ_{2j} are functions of (t,x). It is convenient to decompose these functions in terms of a complete basis. A natural basis is provided by the AdS_{d+1} massless scalar eigenvalues and eigenfunctions (which we refer to from now on as *oscillons*)

$$\omega_j = d + 2j \,, \quad e_j(x) = d_j \, \cos^d x \, {}_2F_1\left(-j, d+j, \frac{d}{2}, \sin^2 x\right) \,, \quad j = 0, 1, \cdots,$$
$$(5.2)$$

where d_j are normalization constants such that

$$\int_0^{\pi/2} dx \, e_i(x) e_j(x) \tan^{d-1} x = \delta_{ij} \,. \tag{5.3}$$

A remarkable observation of [1] was that initial conditions which represent at a linearized level (at order $\mathcal{O}(\epsilon)$) a superposition of several oscillons with different index j appear to be unstable at time scales $t_{\text{instability}} \sim \mathcal{O}(\epsilon^{-2})$; on the other hand, nonlinear effects of a single oscillon do not lead to destabilization. Specifically, the instabilities occur whenever oscillons with indices[4] $\{j_1, j_2, j_3\}$ are present at order $\mathcal{O}(\epsilon)$, while the oscillon with index j_r, such that

$$\omega_{j_r} = \omega_{j_1} + \omega_{j_2} - \omega_{j_3} \,, \tag{5.4}$$

is not excited at this order.

In what follows we argue that the basic conclusion of [1] remains valid even for configurations with $Q \neq 0$. We point out though an interesting twist: although any *finite* number of distinct-index oscillons excited at order $\mathcal{O}(\epsilon)$ leads to nonlinear instabilities at order $\mathcal{O}(\epsilon^3)$, $\mathcal{O}(\epsilon)$ initial configurations with an *infinite* number of distinct-index oscillons remain (formally) stable at order $\mathcal{O}(\epsilon^3)$.

---

[4]The indices could be repeated.

While it is straightforward to carry out the analysis in full generality, to be maximally explicit we discuss the case of $d = 3$ and a superposition of two lowest-frequency oscillons at a linearized level, namely e_0 and e_1. We discuss different cases:

- a single neutral oscillon

- a superposition of two neutral oscillons

- a single charged oscillon

- a superposition of two charged oscillons

- a superposition of a charged and a neutral oscillon.

Lastly, we comment on nonlinear instabilities at $\mathcal{O}(\epsilon^3)$ arising from different channels (5.4), *i.e.*, different combinations of $\{j_1, j_2, j_3\}$ resulting in the same ω_{j_r}).

To distinguish neutral and charged initial conditions it is convenient to express the charge Q given by (2.18) as

$$Q = 4\pi^2 \int_0^{\pi/2} dx \, \tan^2 x \, A^{-1}(t, x) \, e^{\delta(t,x)} \, (\partial_t \phi_1(t, x)\phi_2(t, x) - \partial_t \phi_2(t, x)\phi_1(t, x)) \,.$$

(5.5)

5.1.1 A single neutral oscillon

Here we take

$$\phi_2(t, x) \equiv \phi_1(t, x) \,, \qquad \phi_1(0, x) = \epsilon \, e_0(x) + \mathcal{O}(\epsilon^3) \,, \qquad \partial_t \phi_1(0, x) = 0 \,. \quad (5.6)$$

Clearly, in this case $Q = 0$. Requiring normalizability and regularity of ϕ_1, to order $\mathcal{O}(\epsilon^3)$ (where first nonlinear effects appear), we find

$$\phi_1 = \epsilon \left[e_0(x) \, \cos\left(\left(3 - \frac{135}{4\pi}\epsilon^2\right)t\right)\right] + \epsilon^3 \left[F_{3,3}(x) \, \cos(3t) \right. \\
\left. + F_{3,9}(x) \, \cos(9t)\right] + \mathcal{O}(\epsilon^5) \,,$$

(5.7)

with

$$F_{3,3} = \frac{3\sqrt{2}\cos^3 x}{\pi^{3/2}}\left(12\cos^8 x - 88\cos^6 x + 108\cos^4 x - 63\cos^2 x + 63\pi^2 \right. \\
\left. - 252x^2 - 252x\cot x(2 - \cos^2 x)\right),$$

(5.8)

15

$$F_{3,9} = \frac{4\sqrt{2}}{\pi^{3/2}} \cos^9 x (9 \cos^2 x - 4) \,. \tag{5.9}$$

Notice that in (5.7) we absorbed a term linearly growing in time

$$\propto \epsilon^3 t \sin(\omega_0 t)$$

into $\mathcal{O}(\epsilon^2)$ shift of the leading-order oscillon frequency ω_0:

$$\omega_0 \to w_0 - \frac{135}{4\pi} \epsilon^2 \,. \tag{5.10}$$

Obviously, we could do so because an oscillon with such a frequency has already been present in the initial condition (5.6). For this initial configuration the instability condition (5.4) is satisfied only for $j_1 = j_2 = j_3 = j_r = 0$.

5.1.2   A superposition of two neutral oscillons

Consider now a slightly more general (neutral) initial condition

$$\phi_2(t, x) \equiv \phi_1(t, x) \,, \qquad \phi_1(0, x) = \epsilon \left(e_0(x) + e_1(x) \right) + \mathcal{O}(\epsilon^3) \,, \qquad \partial_t \phi_1(0, x) = 0 \,. \tag{5.11}$$

Once again, in this case $Q = 0$. Requiring normalizability and regularity of ϕ_1, to order $\mathcal{O}(\epsilon^3)$, we find

$$\phi_1 = \epsilon \left[e_0(x) \, \cos\left(\left(3 - \frac{335}{2\pi} \epsilon^2 \right) t \right) + e_1(x) \, \cos\left(\left(5 - \frac{1519}{6\pi} \epsilon^2 \right) t \right) \right] +$$
$$\epsilon^3 \left[\sum_{k=1}^{8} F_{3,2k-1}(x) \, \cos((2k-1)t) + \frac{\sqrt{6}\pi}{105} e_2(x) \, t \, \sin(7t) \right] + \mathcal{O}(\epsilon^5) \,, \tag{5.12}$$

where $F_{3,2j+1}(x)$ are some analytically determined functions[5]. Here, we have three different terms at order $\mathcal{O}(\epsilon^3)$, which grow linearly with time

$$\propto \epsilon^3 t \times \left\{ \cos(\omega_0 t) \,, \; \cos(\omega_1 t) \,, \; \sin(\omega_2 t) \right\} \,. \tag{5.13}$$

The presence of $j = \{0, 1\}$ oscillons in order $\mathcal{O}(\epsilon)$ initial conditions allows us to absorb the first two terms into the shifts of the leading-order oscillon frequencies

$$\omega_0 \to w_0 - \frac{335}{3\pi} \epsilon^2 \,, \qquad \omega_1 \to w_1 - \frac{1519}{6\pi} \epsilon^2 \,. \tag{5.14}$$

We cannot do the same with the remaining term in (5.13) — for this to happen $\phi_1(0, x)$ must contain a term $\propto \epsilon \, e_2(x)$. Of course, the presence of

---

[5]We omit their explicit expressions to keep formulae readable.

$e_2(x)$ at order $\mathcal{O}(\epsilon)$ in the initial conditions, while eliminating $\epsilon^3 t \times \sin(\omega_2 t)$ term, would generate new resonances at $j > 2$. Thus, the absence of linearly growing with time terms at order $\mathcal{O}(\epsilon^3)$ necessitates the excitation of *all* oscillons at order $\mathcal{O}(\epsilon)$ in the initial condition. In what follows we show that $\mathcal{O}(\epsilon^3)$ instabilities can be removed by shifting the leading-order oscillon frequency (provided the relevant excitation is present at order $\mathcal{O}(\epsilon)$), even if they arise from different channels (5.4).

5.1.3 A single charged oscillon

For charged initial data we take

$$\begin{aligned}
\phi_1(0, x) &= \epsilon e_0(x) + \mathcal{O}(\epsilon^3), \qquad \partial_t \phi_1(0, x) = 0, \\
\phi_2(0, x) &= 0, \qquad \partial_t \phi_2(0, x) = \epsilon \omega_0 \; e_0(x) + \mathcal{O}(\epsilon^3),
\end{aligned} \tag{5.15}$$

where (see (5.5))

$$Q = -12\pi^2 \epsilon^2 + \mathcal{O}(\epsilon^4). \tag{5.16}$$

Initial data (5.15) is a direct *charged* generalization of a single-oscillon initial data (5.6). In this case, to order $\mathcal{O}(\epsilon^3)$, we find

$$\begin{aligned}
\phi_1 &= \epsilon \left[e_0(x) \cos\left(\left(3 - \frac{63}{2\pi}\epsilon^2 \right) t \right) \right] + \epsilon^3 \left[F_{3,3}^1(x) \; \cos(3t) \right] + \mathcal{O}(\epsilon^5), \\
\phi_2 &= \epsilon \left[e_0(x) \sin\left(\left(3 - \frac{63}{2\pi}\epsilon^2 \right) t \right) \right] + \epsilon^3 \left[F_{3,3}^2(x) \; \sin(3t) \right] + \mathcal{O}(\epsilon^5).
\end{aligned} \tag{5.17}$$

All the linearly with time growing terms are absorbed into the higher-order shift of ω_0.

5.1.4 A superposition of two charged oscillons

For charged initial data we take

$$\begin{aligned}
\phi_1(0, x) &= \epsilon(e_0(x) + e_1(x)) + \mathcal{O}(\epsilon^3), \qquad \partial_t \phi_1(0, x) = 0, \\
\phi_2(0, x) &= 0, \qquad \partial_t \phi_2(0, x) = \epsilon(\omega_0 \; e_0(x) + \omega_1 \; e_1(x)) + \mathcal{O}(\epsilon^3),
\end{aligned} \tag{5.18}$$

where (see (5.5))

$$Q = -32\pi^2 \epsilon^2 + \mathcal{O}(\epsilon^4). \tag{5.19}$$

17

Initial data (5.18) is a direct *charged* generalization of the two-oscillon initial data (5.11). In this case, to order $\mathcal{O}(\epsilon^3)$, we find

$$\phi_1 = \epsilon \left[e_0(x) \cos\left(\left(3 - \frac{159}{\pi}\epsilon^2 \right) t \right) + e_1(x) \cos\left(\left(5 - \frac{2201}{9\pi}\epsilon^2 \right) t \right) \right]$$

$$+ \epsilon^3 \left[\sum_{k=1}^{4} F_{3,2k-1}^1(x) \cos((2k-1)t) + \frac{50\sqrt{6}}{3\pi} e_2(x) \ t \ \sin(7t) \right] + \mathcal{O}(\epsilon^5),$$

$$\phi_2 = \epsilon \left[e_0(x) \sin\left(\left(3 - \frac{159}{\pi}\epsilon^2 \right) t \right) + e_1(x) \sin\left(\left(5 - \frac{2201}{9\pi}\epsilon^2 \right) t \right) \right]$$

$$+ \epsilon^3 \left[\sum_{k=1}^{4} F_{3,2k-1}^2(x) \sin((2k-1)t) - \frac{50\sqrt{6}}{3\pi} e_2(x) \ t \ \cos(7t) \right] + \mathcal{O}(\epsilon^5).$$

$$(5.20)$$

Parallel to the discussion in Section 5.1.2, the absence of leading order $\propto \epsilon e_2(x)$ modes in the initial condition (5.18) leads to growing resonance terms

$$\propto \epsilon^3 t \times \left\{ \cos(\omega_2 t), \ \sin(\omega_2 t) \right\}. \qquad (5.21)$$

5.1.5   A superposition of a charged oscillon with a neutral one

For charged initial data we take

$$\phi_1(0, x) = \epsilon(e_0(x) + e_1(x)) + \mathcal{O}(\epsilon^3), \qquad \partial_t\phi_1(0, x) = 0,$$
$$\phi_2(0, x) = 0, \qquad \partial_t\phi_2(0, x) = \epsilon\omega_0 \ e_0(x) + \mathcal{O}(\epsilon^3),$$

$$(5.22)$$

where (see (5.5))

$$Q = -12\pi^2\epsilon^2 + \mathcal{O}(\epsilon^4). \qquad (5.23)$$

In this case, to order $\mathcal{O}(\epsilon^3)$ we find

$$\phi_1 = \epsilon \left[e_0(x) \cos\left(\left(3 - \frac{787}{8\pi}\epsilon^2 \right) t \right) + e_1(x) \cos\left(\left(5 - \frac{1843}{12\pi}\epsilon^2 \right) t \right) \right]$$

$$+ \epsilon^3 \left[\sum_{k=1, k \neq 5}^{8} F_{3,2k-1}^1(x) \cos((2k-1)t) + \frac{35\sqrt{6}}{4\pi} e_2(x) \ t \ \sin(7t) \right] + \mathcal{O}(\epsilon^5),$$

$$\phi_2 = \epsilon \left[e_0(x) \sin\left(\left(3 - \frac{153}{2\pi}\epsilon^2 \right) t \right) \right] + \epsilon^3 \left[\sum_{k=1, k \neq 5}^{7} F_{3,2k-1}^2(x) \sin((2k-1)t) \right.$$

$$\left. - \frac{75}{8\pi} e_1(x) \ t \ \cos(5t) + \frac{5\sqrt{6}}{12\pi} e_2(x) \ t \ \cos(7t) \right] + \mathcal{O}(\epsilon^5).$$

$$(5.24)$$

18

Parallel to the discussion in Section 5.1.2, the absence of leading order $\propto \epsilon e_2(x)$ modes in the initial condition (5.22) for both ϕ_1 and ϕ_2 leads to growing resonance terms

$$\propto \epsilon^3 t \times \left\{ \cos(\omega_2 t) \,, \ \sin(\omega_2 t) \right\} . \tag{5.25}$$

Likewise, the absence of a leading order $\propto \epsilon e_1(x)$ mode in the initial condition (5.22) for ϕ_2 leads to a growing resonance term

$$\propto \epsilon^3 t \ \cos(\omega_1 t) . \tag{5.26}$$

5.1.6 Multi-channel instabilities at $\mathcal{O}(\epsilon^3)$ and their removal

Previously, we considered the linear (order $\mathcal{O}(\epsilon)$) superposition of two neutral/charged oscillons and identified instabilities at order $\mathcal{O}(\epsilon^3)$ arising from the resonance term with index j_r (see (5.4)). Furthermore, we showed that if an oscillon $e_{j_r}(x)$ is present in the initial data at order $\mathcal{O}(\epsilon)$, these instabilities can be removed with an appropriate $\mathcal{O}(\epsilon^2)$ shift of the oscillon frequency

$$\omega_{j_r} \to \omega_{j_r} + \epsilon^2 \omega_{j_r}^{(1)} . \tag{5.27}$$

Thus, it appears that to avoid $\mathcal{O}(\epsilon^3)$ instabilities, initial data at order $\mathcal{O}(\epsilon)$ must contain all oscillons.

In all examples discussed, only a single instability channel was present. If all oscillons are excited at order $\mathcal{O}(\epsilon)$, the same resonance frequency w_{j_r} (5.4) would arise from different channels. We argue here that all such multi-channel instabilities can still be removed with a single resonance frequency shift (5.27). To be maximally explicit, consider a neutral, order $\mathcal{O}(\epsilon)$, initial data containing oscillons $j = \{0, 1, 2, 3\}$

$$\phi_2(t, x) \equiv \phi_1(t, x) \,, \qquad \phi_1(0, x) = \epsilon \sum_{j=0}^{3} A_j e_j(x) + \mathcal{O}(\epsilon^3) \,, \qquad \partial_t \phi_1(0, x) = 0 \,,$$
$$\tag{5.28}$$

where A_j are generically different amplitudes. Consider a resonance index $j_r = 2$. From (5.4) there are 7 distinct instability channels:

$$
\begin{aligned}
&(1): \ \omega_{j_r} = \omega_2 + \omega_0 - \omega_0 \,, &\quad &(2): \ \omega_{j_r} = \omega_2 + \omega_1 - \omega_1 \,, \\
&(3): \ \omega_{j_r} = \omega_2 + \omega_2 - \omega_2 \,, &\quad &(4): \ \omega_{j_r} = \omega_2 + \omega_3 - \omega_3 \,, \\
&(5): \ \omega_{j_r} = \omega_1 + \omega_1 - \omega_0 \,, &\quad &(6): \ \omega_{j_r} = \omega_3 + \omega_0 - \omega_1 \,, \\
&(7): \ \omega_{j_r} = \omega_3 + \omega_1 - \omega_2 \,.
\end{aligned}
\tag{5.29}
$$

Each of the channels in (5.29) would contribute a term that grows linearly

with time at order $\mathcal{O}(\epsilon^3)$ to ϕ_1

$$\delta\phi_1^{\text{resonance}} = \epsilon^3 t \sin(\omega_2 t) \; e_2(x) \; \frac{1}{\pi} \left(\frac{60613}{120} A_7^3 + \frac{35\sqrt{6}}{2} A_3 A_5^2 + \frac{189\sqrt{5}}{4} A_3 A_9 A_5 \right.$$

$$\left. + \frac{50607}{40} A_9^2 A_7 + \frac{1090}{3} A_5^2 A_7 + \frac{1797}{20} A_3^2 A_7 + \frac{159\sqrt{30}}{2} A_5 A_7 A_9 \right).$$

$$(5.30)$$

A resonance frequency shift (5.27) would additionally contribute

$$\delta\phi_1^{\text{shift}} = \epsilon^3 t \sin(\omega_2 t) \; e_2(x) \; \frac{1}{\pi} \left(A_7 w_2^{(1)} \right). \qquad (5.31)$$

Clearly, provided $A_7 \neq 0$, all the instabilities (5.29) can be removed, *i.e.*

$$\delta\phi_1^{\text{resonance}} + \delta\phi_1^{\text{shift}} = 0 \, ,$$

for suitably adjusted $w_2^{(1)}$.

Straightforward, but quite tedious, considerations show that for a generic neutral initial condition

$$\phi_2(t,x) \equiv \phi_1(t,x) \, , \qquad \phi_1(0,x) = \epsilon \sum_{j=0}^{\infty} A_j e_j(x) + \mathcal{O}(\epsilon^3) \, , \qquad \partial_t \phi_1(0,x) = 0 \, ,$$

$$(5.32)$$

the presence of resonance contributions from channels

$$\omega_{j_r} = \omega_{j_1} + \omega_{j_2} - \omega_{j_3} \, , \qquad (5.33)$$

can be eliminated by the following resonance frequency shift

$$\omega_{j_r} \rightarrow \omega_{j_r} + \epsilon^2 \sum_{\{j_1,j_2,j_3\}} \frac{A_{j_1} A_{j_2} A_{j_3}}{A_{j_r}} \times \mathcal{O}(1) \, , \qquad (5.34)$$

where summation occurs over all possible instability channels (triplets $\{j_1, j_2, j_3\}$ satisfying (5.33)). The amplitudes A_j are expected to decay fast enough as $j \rightarrow \infty$ for the sum in (5.34) to be convergent[6] (and also not to have an apparent horizon already present at the initial hypersurface).

To reiterate, the reason why renormalization of the basic resonance frequencies ω_{j_r} would remove all instabilities up to order $\mathcal{O}(\epsilon^3)$ is because to this order the necessary frequency shifts due to distinct instability channels (5.33) add-up linearly, as explicitly demonstrated by example (5.28). From the latter example it is also clear that the 'strength' of each of such shifts—$\omega_2^{(1)}$ in equation (5.31)—is inversely proportional to the amplitude of a resonance

---

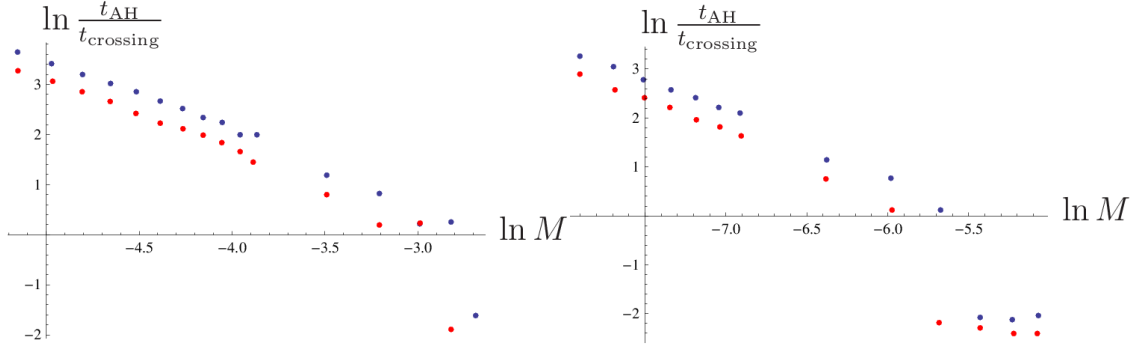[6]In [13] we present an explicit example where this is the case.

Figure 6: AH formation time t_{AH} a function of mass M for $d = 3$ (left panel) and $d = 4$ (right panel) on a log-log plot. The blue dots correspond to thermalization of states with $Q = 0$; the red dots correspond to thermalization of states with $Q \neq 0$. In both cases, for small M (or ϵ), we find that AH is formed earlier than $\propto M^{-1}$ (or $\propto \epsilon^{-2}$) as suggested by weakly nonlinear analysis. A global charge Q of the initial configurations (2.24) does not extend the thermalization time, compared to the same-mass $Q = 0$ configurations (2.23).

frequency at order $\mathcal{O}(\epsilon)$, *i.e.*, $\propto \frac{1}{A_{j_r}}$. Thus, provided all resonances are excited at $\mathcal{O}(\epsilon)$ (so that this 'inverse amplitude strength' is finite), the instabilities can always be eliminated as (schematically) indicated by (5.34).

Note that while we discussed neutral initial conditions, similar considerations also apply for initial conditions carrying global charge. Whether or not weakly-nonlinear instabilities can be removed (or removed under some conditions) beyond order $\mathcal{O}(\epsilon^3)$ is an interesting open question. We emphasize that our numerical simulations, as well as those reported in [1, 2] are outside the weakly nonlinear regime.

5.2 Global charge and the thermalization time

In global AdS_d, the time it takes for a null geodesic to cross the space-time is

$$t_{\mathrm{crossing}} = \pi \,. \tag{5.35}$$

In Fig. 6 we present the ratio of the AH formation time t_{AH} to t_{crossing} as a function of mass M. The blue dots represent collapse from initial condition (2.23), and the red dots correspond to collapse from initial condition (2.24). We find that an AH is forming earlier for $Q \neq 0$ initial conditions
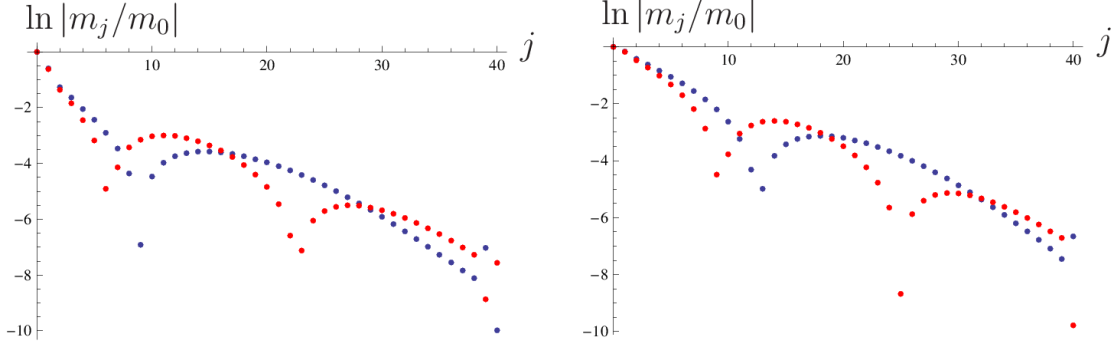
Figure 7: Decomposition of the mass aspect function $\mathcal{M}(t = 0, x)$ into the oscillon basis for two contrasting initial configurations: for $\epsilon = 10$ neutral (2.23) initial condition (blue dots), and the charged initial condition (2.24) with the same mass (red dots). Left panel: $d = 3$, right panel: $d = 4$. The different spectra in the oscillon basis do not appear to account for the difference in the observed AH formation times.

with the same mass as the corresponding $Q = 0$ initial conditions. This difference in collapse times could potentially be attributable to either: (i) that one has a global charge while the other is neutral, or (ii) that the spectral content of the two initial conditions are different. To understand which of these is responsible, we decompose the mass aspect function (2.20) into the oscillon basis (5.2)

$$\mathcal{M}(t = 0, x) = \sum_{j=0}^{\infty} m_j \, e_j(x) \,. \tag{5.36}$$

The spectral content for the two initial conditions (both with the same mass) is presented in Fig. 7. The spectrum of the charged configuration does *not* show a noticeably broader bandwidth or enhanced amplitudes at high frequencies when compared to the spectrum of the neutral configuration. Thus, it appears that the acceleration of the collapse is a dynamical effect related to the class of initial conditions (2.24).

In a similar fashion, we find significant differences in collapse times when changing the spacetime dimensions d. However, in this case the spectral content of the initial mass aspect function *does* account for the difference in AH formation time. The left panel in Fig. 8 compares AH formation times for $d = 3$ (blue dots) and $d = 4$ (red dots). The spectral content of the corresponding mass aspect function is shown in the right panel. Because higher dimensional oscillons are more localized in the AdS_{d+1} center with
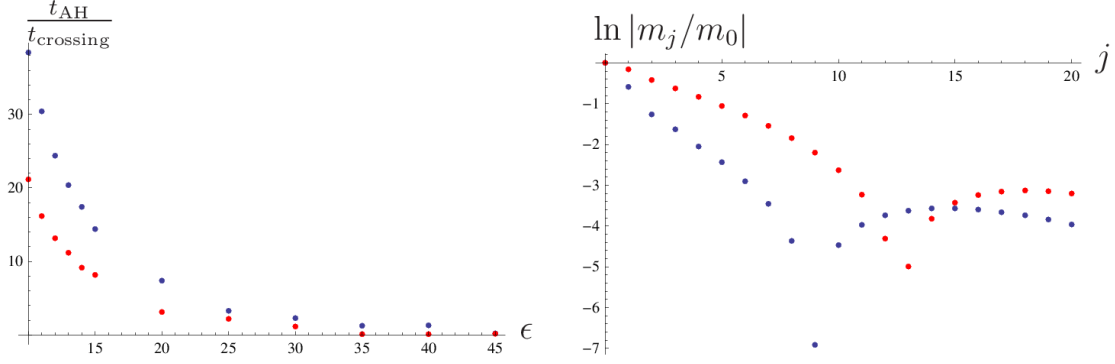
22

Figure 8: The AH formation time noticeably decreases with increasing boundary space-time dimension d (left panel). Blue dots represent $d = 3$ and red dots $d = 4$. This decrease can be explained by the broadening of the oscillon decomposition spectrum (see (5.36)) of the mass aspect function corresponding to initial conditions for different d (right panel).

increasing d, there is larger overlap of the initial profile (2.23) with higher modes for larger d, resulting in broadening of the spectral bandwidth.

5.3 Bulk vs boundary turbulence

A motivating question behind this study wonders what the CFT sees of this instability on the boundary. Because the only observables on the boundary we consider are the (unchanging) total mass M and the asymptotic behavior of the scalar fields $\phi_d^{(i)}(t)$ (see (2.15)) (or equivalently $\langle \mathcal{O}_d^{(i)} \rangle$, see (2.16)), we examine the spectral content of the latter.

Fig. 5 displays snapshots of the scalar field for successive bounces during an evolution. The initial pulse becomes increasingly more compact, approaching something like a Kronecker delta function. As it does so, the FFT of each pulse similarly approaches the FFT of a delta function, in particular, a flat, plateau-like spectrum. In general, if we define the effective bandwidth of the power spectrum as the frequency at which the plateau ceases, then we observe this bandwidth to increase rapidly during an evolution. The only exception appears, for some runs, during the last few bounces, during which the bandwidth decreases modestly from its maximum. However, we speculate that this behavior can be attributed to the nonlinearities of gravity near black hole formation.

Before discussing the behavior of the bandwidth, we should comment on

23

the falloff behavior of the power spectrum. It is customary in studies of turbulence in fluid dynamics to observe the rate of falloff (the slope on a log-log plot). In particular, a famous result of Kolmogorov expects a slope in the *energy spectra* of $-5/3$ within the inertial regime of turbulent flows (independent of spatial dimension d). Here, one might consider the scalar field, in analogy with a fluid, as a "gas" of oscillons in which structure transitions to increasingly higher frequencies. An analysis of the energy spectra over the oscillon basis in the bulk in [17] finds a fall-off at the rate of -1.22. As well, an analysis of the Fourier spectrum over the time series of the Ricci scalar at the origin in [19] reports a slope of -1.61, seemingly close to that of Kolmogorov. However, the Ricci scalar is an energy density and thus the expected scaling is not $-5/3$. Indeed, we can retrace Kolmogorov's argument for such quantity by the following dimensional considerations. The Fourier transform of Π^2 (which scales as $\mathcal{E} \propto T^{-2}$) scales as $\hat{\mathcal{E}} \propto LT^{-2}$ for a typical wavelength L. If turbulent behavior transfers energy to different scales, for Π^2 it does so with an efficiency η which has dimensions of T^{-3} (transfer per unit time). Thus, one would expect these quantities to be related by

$$\hat{\mathcal{E}} \equiv \left[\frac{L}{T^2}\right] = \eta^p \omega^\alpha \equiv \left[\frac{1}{T^3}\right]^p \left[\frac{1}{L}\right]^{-\alpha} , \tag{5.37}$$

where p and α are (so far) arbitrary powers. However, for (5.37) to be dimensionally consistent, then we must have $p = 2/3$ and and $\alpha = -1$.

In evaluating what our data says about the falloff, we have to know which parts of the spectrum represent true physics as opposed to numerical noise. Straightforward unigrid convergence tests suggests that we can roughly trust the spectra up to a bit better than $\omega \approx 500$ (i.e. the Nyquist frequency $\omega_N = \pi/(2\Delta x)$ with Δx the grid spacing). However, in general, we run with AMR and can resolve locally enormously better than any of our unigrid evolutions. One issue is that while AMR is very efficient locally, its performance on global measures is difficult to evaluate. Instead, we carryout some runs with different AMR parameters and evaluate where the spectrum changes significantly.

Additionally, AMR introduces its own noise into the asymptotic behavior of the scalar field, especially for higher dimensions ($d \geq 6$). This noise appears as very small kinks in the time series data which contribute noise that behaves as $\propto \omega^{-2}$ (such that the power fall-off from this noise source is -4).

We also note two other sources of noise in the spectrum. In order to carryout a Fourier decomposition, we first interpolate to a grid uniform in t. Comparing FFTs with either linear or cubic interpolation, we find this noise is generally small, only significant at quite high frequencies and not strongly dependent on the interpolation order. The final source of noise

arises from potential mismatches in the time-series data between $\phi_d^{(i)}(n\pi)$ and $\phi_d^{(i)}([n+1]\pi)$. Because the FFT expects a periodic signal, this mismatch appears as a (quite small) discontinuity producing noise that falls off as $\propto \omega^{-1}$ (with a power that falls off with exponent -2).

As a practical matter, we find that for different runs, different noise sources dominate the high-frequency behavior of the power spectrum. Indeed the only robust features of the various power spectra we have computed at the AdS boundary have been the delta-function plateau and high-frequency noise the power of which falls off either with slope -2 or -4. In particular, to make a convincing argument that some particular fall-off is characteristic of this weakly nonlinear instability, one needs to demonstrate not only a feature of the spectrum independent of any noise, but also a feature not present in the initial spectrum. That is, any characteristic feature must *develop* from the evolution.

At the boundary, the only such feature we find is that of the plateau and we study its defining feature, its bandwidth. In Fig. 9, we display the results of measuring the bandwidth for one set of evolutions. We show the power spectrum of the first, middle, and last bounces. From each bounce, we calculate a maximum frequency as the location where the spectral power falls some threshold below the maximum (typically 20% below the maximum). This frequency then serves as an estimate of the bandwidth of the pulse and is shown on the right side of the figure. As the pulse sharpens in time, its spectrum reaches into higher frequencies and the rate at which it does so is roughly exponential.

Looking at the right side of Fig. 9, one notices that the growthrate of the bandwidth, after an initial quiescent period, appears to approach a line, representing exponential growth of the bandwidth. We are thus led to examine the bandwidth of runs with a relatively large number of bounces, and indeed we find exponential growth of the bandwidth for these runs, shown in Fig. 10.

What is particularly interesting about Fig. 10 is that these runs demonstrate what appears to be a common growth rate with slope 0.04. This commonality in slope appears despite the fact that these families span different dimensions d and different forms of initial data. What they have in common is that they all form black holes after between 26 and 39 bounces. Note that the growth rate for these evolutions differs from that shown for $d = 3$ in Fig. 9 (with a slope of roughly 0.07) which collapses after just 21 bounces.

Another interesting aspect of these bandwidth-vs-bounce plots is that nearly all evolutions studied terminate at roughly $\log_{10}(\Delta\omega) \approx 2.7$. Presumably this reflects that black hole formation occurs for such high-frequencies. We speculate based on these two features, that a bandwidth plot such as

discussed here can be considered as something of a phase-space picture for this system. At the top of the plot, is black hole formation. Low on the left side, evolutions not yet consisting of a black hole evolve through some quiescent period. Depending on how weak the initial data, they enter an exponentially growing bandwidth regime until they are brought to black hole formation. Perhaps, the growth rate in this linear regime is set by how low they begin, or, equivalently, how many bounces they require to achieve the black hole scale. We stress that this is speculation and will require more runs to test whether indeed common growth rates occur for disparate evolutions that share the same number of bounces. Similarly, this phase space picture may require some other basis, such as the oscillon basis, over which to compute the bandwidth.

Last, we also monitor the behavior of Π^2 *at the origin* which is related to the energy density (and scales in the same way). Numerically, the behavior of the scalar fields at the origin produces less noise and hence cleaner power spectra. Figure 11 presents results for $d = 3, 4, 5$, and 6 for the last bounce before black hole formation. At frequencies below $\omega \simeq 800$ a plateau behavior results from the pulse profile being quite narrow and approaching a delta-like behavior. Within the range $\omega \in (800, 3000)$ the slopes measured fall in the interval $\approx (-1.8, -2.2)$, consistent with our previous Kolmogorov-type argument for the power spectrum of a quantity scaling as energy density (recall that the *power* spectrum is the square of the complex Fourier amplitude and hence should fall-off as -2α).

The relatively wide range of this interval is perhaps not surprising given that we lack sharp knowledge of where the inertial regime lies in the spectrum[7]. On one hand, because energy is only "injected" initially, as it shifts to higher frequencies it pushes the initial lower bound for the inertial frequency higher. On the other hand, at high frequencies one has a "dissipative" scale determined by the black hole size. However, because energy is also "spent" in curving the spacetime, the location of this dissipative bound is also difficult to determine. Nevertheless, inspection of slope breaks in the low and high frequency regimes leave an intermediate domain in which the power spectra appears to fall-off with a slope in the range mentioned. Pushing the analogy with turbulent fluid dynamics even further, one could speculate that deviations from a slope of -2 are not surprising, but instead that they would arise much as *intermittency* arises in turbulent fluids. With fluids, intermittency introduces deviations from the $-5/3$ slope due to the presence and dynamics of vortices. Here perhaps the sharpening pulse as it periodically propagates through the origin could leave a similar imprint on the spectrum.

---

[7]To more easily identify this regime, one could introduce boundary deformations to continuously pump energy from the boundary into the system as done in e.g. [20]
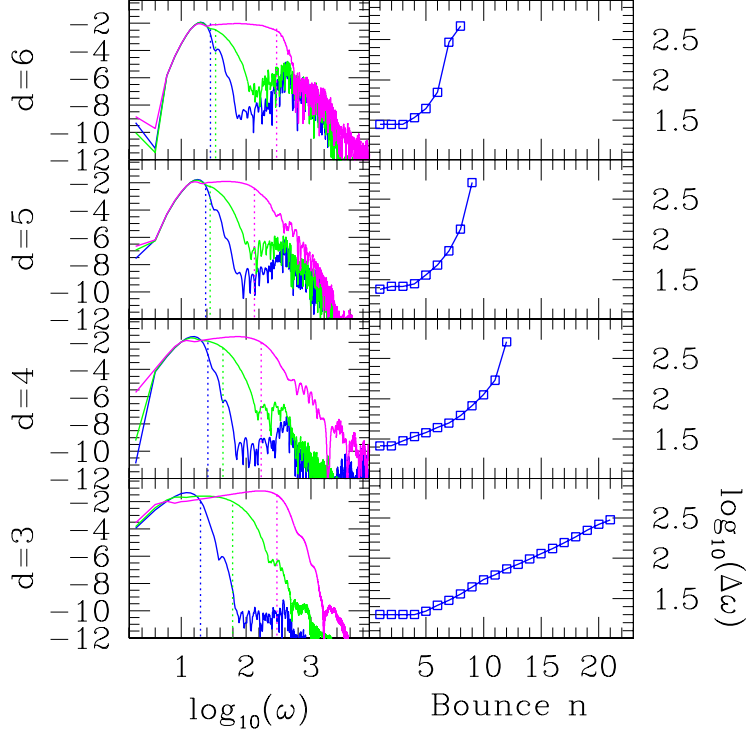
Figure 9: Demonstration of the bandwidth growth with each bounce. Shown are the results from the evolution of initial data of form (2.23) with $\epsilon = 8$, $\sigma = 0.1$ for dimensions $d = 3, 4, 5$ and 6. On the **left** is shown the spectrum of the first (blue), middle (green), and last (magenta) bounces. The pulses increasingly demonstrate a plateau-like region indicative of becoming more like a delta function. At frequencies above the plateau, unphysical noise is apparent. On the **right** is shown the bandwidth associated with all pulses. The bandwidth is obtained as the location at which the spectrum drops from its maximum by twenty percent. As noted in the text (see Fig. 8), the same initial profile for the scalar field contains higher oscillons in its decomposition with higher dimensions, and therefore one observes the bandwidth of the pulses grow more quickly than the $d = 3$ case.
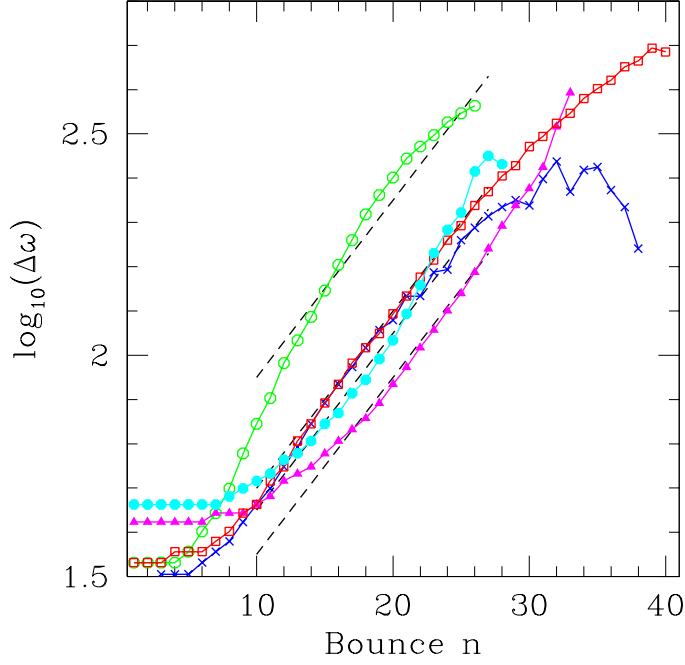
27

Figure 10: Bandwidth as a function of bounce for a few different evolutions. Choosing evolutions with roughly 30 bounces with different dimension d and different families, we observe similar, exponential growth of the bandwidth for some intermediate regime (roughly from bounce 10 to bounce 30). Shown are the results from: (blue crosses) initial configuration (2.23) with $\epsilon = 10$ in $d = 3$, (green open circles) initial configuration (2.24) with $\epsilon = 10$ in $d = 3$, (cyan open circles) initial configuration (2.23) with $\epsilon = 7$ in $d = 6$, (magenta triangles) initial configuration (2.23) with $\epsilon = 7$ in $d = 5$, and (red squares) a Gaussian initial profile in $d = 3$. four (black dashed) lines all with the slope 0.04 but with various y-intercepts chosen to align with the bandwidth data are shown.
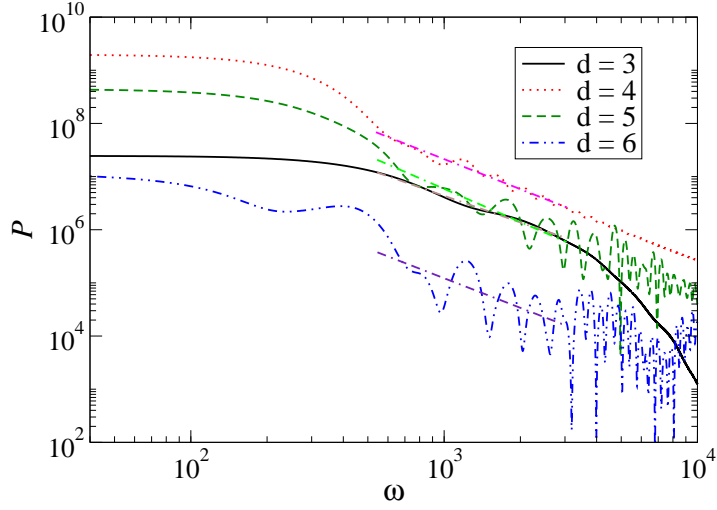
Figure 11: Power spectra of Π^2 at the origin versus frequency ω for $d = 3, 4, 5, 6$ as measured in the last bounce before black hole formation. At frequencies below ≈ 800, the apparent plateau behavior is indicative of the sharpened profile of the pulse. At higher frequencies up to $\omega \approx 3000$, the spectral power decreases with a slope in the range $\in (-1.8, -2.2)$.

6 Conclusion

We have reproduced the work of [1, 2] and provided details of our numerics and tests. We find that this instability towards higher frequencies occurs even in a finite-sized domain with reflecting boundary conditions that would not be expected to know that the spacetime is asymptotically AdS. This result, along with the similar case in asymptotically Minkowski in the work of [17], suggests that the instability is a property not of AdS itself, but instead of gravity in a bounded domain.

We generalized the work of [1, 2] to complex scalar collapse in AdS to address the question of whether AH formation in global AdS from generic initial conditions from the bulk perspective (or thermalization trajectories from the boundary CFT perspective) is sensitive to the presence of a conserved global charge. For the class of initial conditions we study ((2.23) and (2.24)) the answer appears to be "no." Rather, the collapse is affected by the spectral decomposition of the initial data in the oscillon basis (see (5.2)). We would like to stress that global charge can (and does [13]) strongly influence AH formation trajectories in the vicinity of stable stationary configurations in AdS.

We repeated the weakly nonlinear analysis of the gravitational collapse in the oscillon basis, originally presented in [1]. We argued that to the leading order in nonlinearities, all the instabilities can be removed, provided *all* oscillons are excited at the linearized level. This conclusion is robust and independent of the global charge. We further argued that, while the picture of gravitational collapse as an ideal gas of oscillons is valid in the linearized regime, this interpretation is in conflict with the late-time evolution.

Finally, it is clear that gravitational collapse in AdS (or confined gravity) is driven by some focusing mechanism by which the bulk energy density cascades to shorter scales. We have analyzed this behavior from both bulk and boundary perspectives. In the latter, we have uncovered an exponential behavior in the growth of the spectral bandwidth of the scalar field. This observation is also confirmed by examining the behavior at the origin and, interestingly, Π^2 displays a behavior consistent with a Kolmogorov-like mechanism. However, further investigations are required to put this observation on firmer footing.

References

[1] P. Bizon and A. Rostworowski, "On weakly turbulent instability of anti-de Sitter space," *Phys.Rev.Lett.* **107** (2011) 031102, `arXiv:1104.3702 [gr-qc]`.

[2] J. Jalmuzna, A. Rostworowski, and P. Bizon, "A Comment on AdS collapse of a scalar field in higher dimensions," *Phys.Rev.* **D84** (2011) 085021, `arXiv:1108.4539 [gr-qc]`.

[3] F. Pretorius and M. W. Choptuik, "Gravitational collapse in (2+1)-dimensional AdS space-time," *Phys.Rev.* **D62** (2000) 124012, `arXiv:gr-qc/0007008 [gr-qc]`.

[4] D. Garfinkle and L. A. Pando Zayas, "Rapid Thermalization in Field Theory from Gravitational Collapse," *Phys.Rev.* **D84** (2011) 066006, `arXiv:1106.2339 [hep-th]`.

[5] D. Garfinkle, L. A. Pando Zayas, and D. Reichmann, "On Field Theory Thermalization from Gravitational Collapse," *JHEP* **1202** (2012) 119, `arXiv:1110.5823 [hep-th]`.

[6] O. J. Dias, G. T. Horowitz, and J. E. Santos, "Gravitational Turbulent Instability of Anti-de Sitter Space," *Class.Quant.Grav.* **29** (2012) 194002, `arXiv:1109.1825 [hep-th]`.

[7] M. W. Choptuik, "Universality and scaling in gravitational collapse of a massless scalar field," *Phys.Rev.Lett.* **70** (1993) 9–12.

[8] C. Gundlach and J. M. Martin-Garcia, "Critical phenomena in gravitational collapse," *Living Rev.Rel.* **10** (2007) 5, `arXiv:0711.4620 [gr-qc]`.

[9] M. T. Anderson, "On the uniqueness and global dynamics of AdS spacetimes," *Class.Quant.Grav.* **23** (2006) 6935–6954, `arXiv:hep-th/0605293 [hep-th]`.

[10] M. Dafermos. Private communication, (2011).

[11] A. Ishibashi and K. Maeda, "Singularities in asymptotically anti-de Sitter spacetimes," `arXiv:1208.1563 [hep-th]`.

[12] O. J. Dias, G. T. Horowitz, D. Marolf, and J. E. Santos, "On the Nonlinear Stability of Asymptotically Anti-de Sitter Solutions," arXiv:1208.5772 [gr-qc].

[13] A. Buchel, L. Lehner, and S. L. Liebling, "Boson stars in AdS," *in preparation* (2012) .

[14] D. Astefanesei and E. Radu, "Boson stars with negative cosmological constant," *Nucl.Phys.* **B665** (2003) 594–622, arXiv:gr-qc/0309131 [gr-qc].

[15] M. W. Choptuik, "Experiences with an adaptive mesh refinement algorithm in numerical relativity," in *Frontiers in numerical relativity*, C. Evans, L. Finn, and D. Hobill, eds. Cambridge University Press, 1989.

[16] L. Lehner, S. L. Liebling, and O. Reula, "AMR, stability and higher accuracy," *Class.Quant.Grav.* **23** (2006) S421–S446, arXiv:gr-qc/0510111 [gr-qc].

[17] M. Maliborski, "Instability of Minkowski spacetime enclosed in a cavity," arXiv:1208.2934 [gr-qc].

[18] M. Frigo and S. G. Johnson, "Fastest fourier transform in the west (fftw)." http://www.fftw.org/, 2012.

[19] H. de Oliveira, L. A. P. Zayas, and E. Rodrigues, ''A Kolmogorov-Zakharov Spectrum in AdS Gravitational Collapse,'' arXiv:1209.2369 [hep-th].

[20] A. Buchel, L. Lehner, and R. C. Myers, ''Thermal quenches in N=2* plasmas,'' *JHEP* 1208 (2012) 049, arXiv:1206.6785 [hep-th].

32